

GT2011-46044

## DESIGN AND AERODYNAMIC ANALYSIS OF A HIGHLY LOADED HELIUM COMPRESSOR

Tingfeng Ke and Qun Zheng

Harbin Engineering University, Harbin 150001, China  
E-mail: [zhengqun@hrbeu.edu.cn](mailto:zhengqun@hrbeu.edu.cn), [ketingfeng313@126.com](mailto:ketingfeng313@126.com)

### ABSTRACT

A design study of the multistage axial helium compressor of a 300MW nuclear gas turbine is presented in this paper. To design the helium compressor, we apply a new velocity triangle, which is different from that of the conventional air compressor. And the new velocity triangle is of large flow coefficient and negative pre-swirl etc. Comparing with the design based on conventional air compressor technique, the new helium compressor stage loading is increased by nearly three times when inlet flow coefficient increases from 0.6 to 2.04, thus stage numbers could decrease from 16 to 6. The higher loadings result in exacerbated corner separations. An increased reaction can relief the three dimensional separation and achieve the expectant stage pressure ratio. The ratio of the maximum thickness to the chord length of the rotor blade from hub to shroud is optimized and three dimensional profiling is applied. In such a way, the separation in the highly loaded helium compressor channel can be controlled and the optimum efficiency achieved. The performance investigation of the designed stage shows that the highly loaded design has acceptable stall margin.

**Key words: Helium compressor; 3D numerical simulation; highly loaded; separation; globe performance; stall margin**

### INTRODUCTION

High Temperature Gas cooled Reactor (HTGR) could be next generation safe nuclear power plant. For HTGR technology, the power conversion unit currently trend towards utilizing gas turbine generator system because of its high efficiency and simple structure. Several research or practical projects are under planning. For example, the projects of PBMR, GT-MHR, GTHTR300, etc (Matzner, 2004, Kostin et al, 2004, Kunitomi et al, 2004). Japan Atomic Energy Agency's (JAEA's) 300MW High Temperature Gas Cooled Reactor-Gas Turbine (HTGR-GT) power plant has completed the feasibility study. The inlet and outlet gas temperature in the reactor are 550°C and 900 °C respectively. The inlet helium gas pressure is 6MPa. The turbine

system is a recuperative intercooled direct cycle (Yasushi Muto, et al, 2000).

The helium compressor plays an important role in the High Temperature Gas Reactor (HTGR) system as high pressure helium at the designed operating conditions acting as the coolant for the HTGR and as the working fluid for the power conversion unit. The performances of helium compressor depend on the design parameters like those of air compressor. The meridional contour of highly loaded air compressor is strongly converging whereas helium compressor has an almost constant blade height, allowing the use of nearly identical stages from inlet to outlet. This means the design study of a helium compressor can be concentrated on one stage.

The aerodynamic design of a 600MW multistage helium turbine for a high temperature nuclear reactor closed cycle gas turbine has been described by Van den Braembussche<sup>[8]</sup>. Several modifications of the original blades have been made and verified in an attempt to increase the efficiency, such as a redesign of the blade leading edge to create an accelerating flow along the pressure side; an increase of the stator blade number from 58 to 77 and a reduction of the blade chord to keep the pitch to chord ratio constant. These results in a 25% increase of the aspect ratio and reduce the impact of secondary losses on the overall performance. (R. A. Van den Braembussche, 2008)

For a given pressure ratio, the number of stages of a helium compressor is much more than that of an air compressor. That would result in the rotor of a helium compressor being longer and slender, which is of bad rotor dynamics behavior. Rotor dynamics is another technical challenge for helium compressor.

A high reaction stage design could be more effective for helium compressor than an industrial air compressor. The advanced aerodynamic techniques incorporated in the present helium compressor design include the blade-end bows to eliminate flow separation and the blade over-camber to compensate for flow distortion near the end-wall (see Fig. 1d and 1e). These design features are combined with optimum blade row solidity and aspect ratio to attain better efficiency and flow stability (Yan, X. and Takizuka, 2008).

Because the special property of helium, a new velocity triangle may enhance the helium flows (Mihayilufu, 1964). And the new velocity triangle has improved the performance of helium compressor and the stage loading could be increased severalfold in two dimensional cases (Yanli Long, 2008).

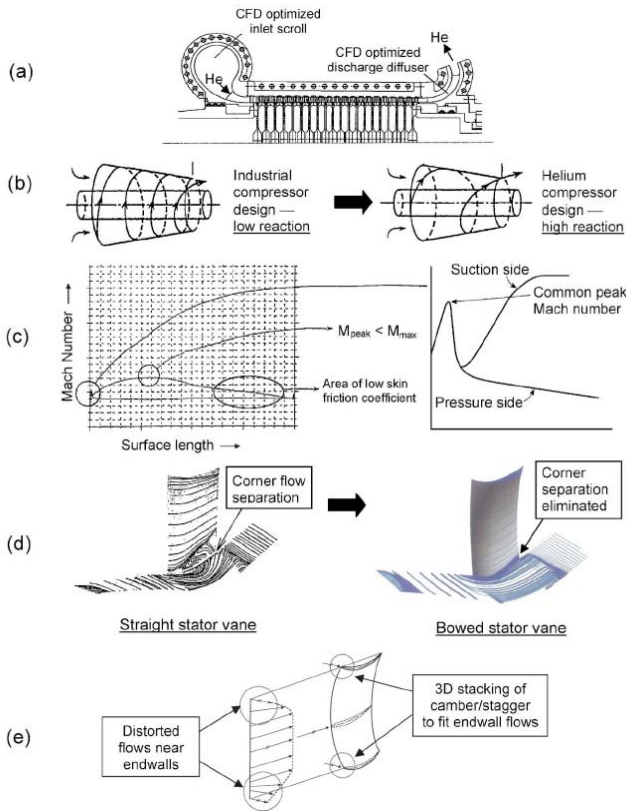


**Figure 1 The present prototype design approach**

Compressing helium to the required pressure is a tough task due to its property (Refer to Table 1), which results in many stages are necessary for the helium compressor, therefore, the investigation of the highly loaded blade airfoil is a key design issue in the development and deployment of helium compressor for high temperature gas cooled reactor. Generally the Mach number is relatively lower in the helium compressor, so a new velocity triangle of helium compressor will be adapted with higher stage loading.

**Table 1 Helium and air physical properties (\*)**

	$C_p$ $kJ / (kg \cdot K)$	$\gamma$	$\rho$ $kg / m^3$	$\mu$ $\mu Pa \cdot s$	$R$ $J / (kg \cdot K)$
Helium	5.23	1.66	0.166	20.0	2077
Air	1.01	1.4	1.205	18.6	287

\* NTP (Normal Temperature and Pressure) is defined as 293.15 K and 1atm (101.325kPa) [4]

In this paper, we try to design a highly-loaded compressor with the new velocity triangle in three-dimensional, and then numerical analysis are carried out to investigate the relationship between the reaction, stage loading and efficiency etc. Due to the serious three dimensional losses, further improvements of

the helium compressor performance can be obtained by advanced aerodynamic design techniques, such as changing the rotor blade load in spanwise and optimizing the maximum thickness of the rotor blade from hub to shroud to achieve the expectant stage pressure ratio. Overall performance has been simulated at design rotational speed and different back-pressures up to helium compressor stall, the steady working range for this highly-loaded helium compressor is investigated.

## DESIGN OF THE HIGHLY LOADED HELIUM COMPRESSOR

The Euler's turbomachine basic equation (Wilson et al, 1998) is:

$$L_u = U \Delta W_u = \psi u^2$$

Increasing the pressure ratio and reducing the number of the stages both require a greater pressure rise per stage. This can be achieved by increasing either the blade speed or the stage loading coefficient. If the blade speed is limited by mechanical constraint then a higher pressure ratio would be required to increase the stage loading.

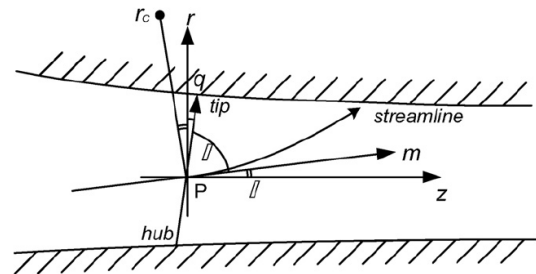


**Figure 2 Meridional view of an axial-flow compressor**

Although stage loading coefficient gives some measures of the stage pressure rise, it is not adequate to describe the aerodynamic performance. Lieblein developed a parameter, which is the first, also the most commonly used to measure the adverse pressure gradient experienced in the suction surface boundary; i.e. the diffusion factor (based on velocity triangles and solidity)

$$D_f = 1 - \frac{W_2}{W_1} + \frac{\Delta W_u}{2W_1 \tau}$$

The velocity triangles that could be used to design helium compressor are shown in Fig. 3(a) and 3(b).

Fig. 3(a) is the velocity triangle of a conventional subsonic air compressor with positive pre-swirl and 0.5 reaction. Although the flow coefficient is big, the turning angle is small, so does the load coefficient. Fig. 3(b) is the new proposed helium velocity triangle with big turning angle and negative pre-swirl. Despite the other parameters are almost the same as the positive pre-swirl one, the turning angle increases a lot, so does the load coefficient. In the following study this new proposed helium velocity triangle will be applied to design helium compressor.

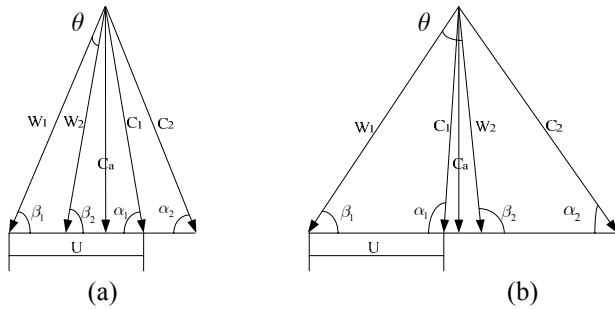


**Figure 3 Velocity triangle of helium compressor**

(a) Possible helium velocity triangle,  
 $\Omega = 0.5$  ;  $\varphi = 2.04$  ;  $\psi = 0.345$

(b) Proposed helium velocity triangle,  
 $\Omega = 0.5$  ;  $\varphi = 2.04$  ;  $\psi = 1.56$

As shown in figure 4, the highly loaded design has increased the axial velocity a lot, results in the  $\Delta W_u$  increasing nearly 3 times. The two velocity triangles have the same reaction 0.7 and blade speed.

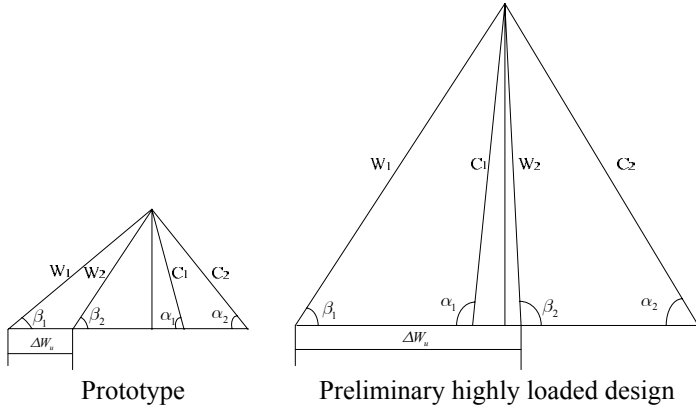


**Figure 4 Comparison triangle velocity of prototype and highly loaded one**

Figure 5 shows the comparison of the blade profile. The geometry of blade profile, such as the chord length, stagger angle, turning angle, maximum thickness..., has changed a lot between based prototype and preliminary highly loaded design.

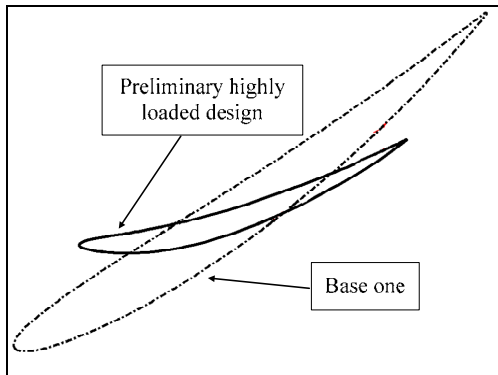


**Figure 5 Prototype design vs. new highly loaded design rotor blade**

The comparison of main design parameters for the first stage of the prototype design and the preliminary highly loaded helium design is shown in table 2.

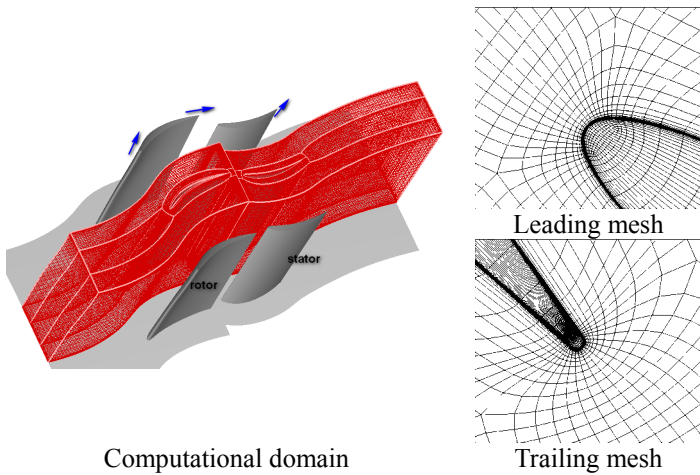
**Table 2 Specification of the helium compressor stage**

Parameters	Prototype design	Preliminary highly loaded design
Inlet pressure [MPa]	2.442	2.442
Inlet temperature [°C]	35	35
Single stage pressure ratio	1.03	1.07
Mass flow [kg/s]	178.2	178.2
Axial velocity[m/s]	154.3	400.0
Aerodynamic design pitch line values		
Number of stages	16	6
Tip diameter (first rotor) [m]	1.426	1.080
Hub diameter (first stator) [m]	1.282	1.000
Tip speed (first stage) [m/s]	268.78	203.67
Rotor/stator vane/blade count (first stage)	142/167	175/200
Rotor/stator chord (first stage) [mm]	41.936/35.586	22.44/19.46
Rotor/stator solidity (first stage)	1.4/1.4	1.2/1.2
Rotor/stator aspect ratio (first stage)	1.7/ 2.0	1.8/2.0
Rotor tip/stator hub clearance	1% blade span	1% blade span
Flow coefficient	0.6	2.04
Load coefficient	0.32	1.42
Reaction	0.7	0.7

## COMPUTATIONAL DETAILS AND SIMULATION RESULTS

The first stage of the designed helium compressor is numerically simulated with commercial Computational Fluid Dynamic (CFD) software package NUMECA. Helium material properties are considered and incorporated into the software. The Navier-Stokes equations are discretized with a cell-centered explicit finite volume scheme according to Jameson in a relative coordinate system rotating together with the reference frame. Time integration is a four-step Runge-Kutta algorithm. In order to speed up the convergence, local time steps, residual smoothing and multigrid techniques were applied. The Spalart-Allmaras turbulence model was used for the closure of the equations. The computational mesh is generated with grid generation tool of NUMECA/Autogrid/IGG. For fulfilling the requirement of the turbulence model,  $y^+$  was controlled within 10. Total grid number of a single blade passage is about 700,000. Figure 4 shows the single stage structure and the medium grids of the computational mesh.

For compressible flows the absolute total quantities (pressure, temperature) and the flow angles are given at the inlet boundary and the static pressure is given at the outlet boundary. This exit pressure can be imposed as an average value at the exit. But in this paper the design must be of accurate mass-flow, an automatic procedure introduces a variation of the imposed exit pressure at every calculational iteration. The pressure is then iteratively updated to convergence in order to reach the imposed mass-flow.



Computational domain  
**Figure 4 Computational mesh**

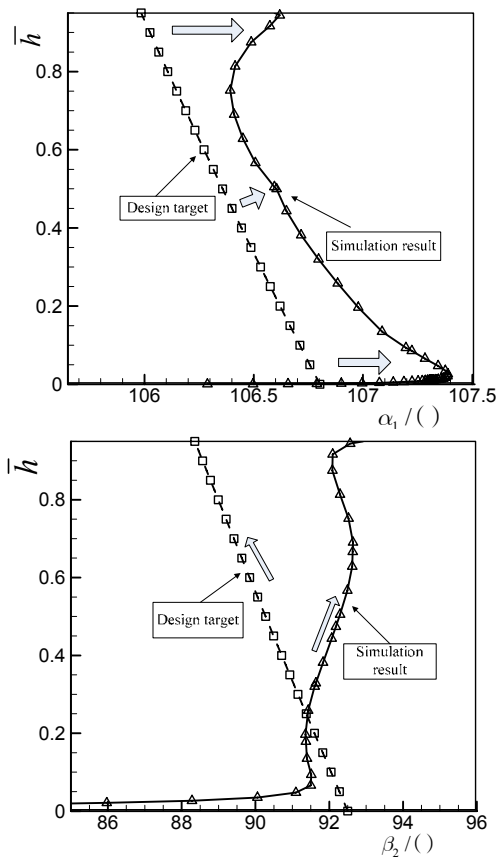


**Figure 5 Comparison of design and CFD results of the pitch-averaged flow angles at rotor inlet and exit**

Figure 5 shows the rotor flow angles distribution in spanwise. As one of the design features of the preliminary highly loaded helium compressor, the rotor inlet absolute angle and rotor outlet relative angle should be generally greater than  $90^\circ$  as proposed in Figure 3, except in the two end-walls boundary layers. And the simulation results are identical with the proposed velocity triangle. Compared with the design target shown as dash line, the simulated inlet angle is a little larger than the target value, especially at two ends. For outlet angle,

the simulated result is smaller than those of designs in 5%-25% height of blade region. While from 25%-100% height of blade, the simulated values become far away from the target values.

The Lieblein diffusion factors  $D_f$  of both the rotor blade and stator vane are below 0.6, the maximum limit value. The preliminary highly loaded helium design is still reasonable from the aerodynamic view. The higher diffusion factors located in the tip area for the stator vane and the higher diffusion factors happened in the hub area for the rotor blade. Special attentions should be paid to these areas, as shown in the figure 6, the diffusion factor  $D_f$  at the rotor hub section is close to 0.6, and large corner separation may happen and has to be controlled.

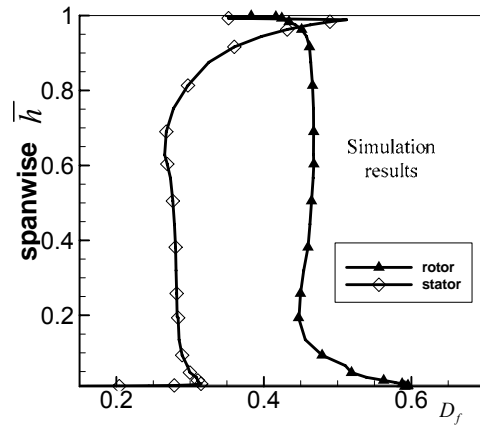


**Figure 6 Lieblein diffusion factor distributions of rotor and stator**

Basically speaking, the preliminary highly loaded design of the first stage is validated by the above simulation results, the main flow features of the compressor stage could be captured by the numerical model used in this research. The new velocity triangle can be applied successfully to increase the helium compressor stage loading. More flow field features need to reveal, from which the improved methods can be found to reduce the flow defect.

As shown in Figure 7, Mach number contour indicates that the highest Mach number is around 0.55 in spite of the highly loaded design with the new velocity triangle. Corner separation happens in the hub area as predicted with diffusion factor in Figure 6. We can find that the rotor suction surface separation line has originated at about 50% chord from the leading edge and terminated at 20% height of the blade. At the end of the separation line on suction surface, a vortex has emerged. At the same time the large corner separation exists at stator suction surface upper part, the tip area.

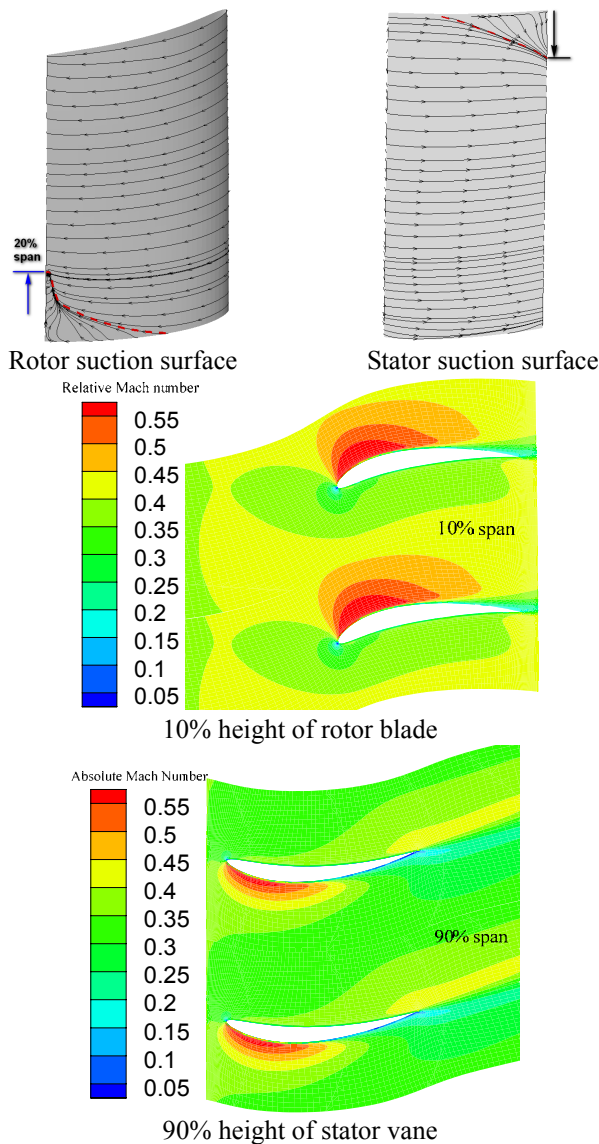


**Figure 7 Streamlines on suction surfaces and Mach number contours of rotor and stator**

Figure 9 demonstrates the radial distribution of the pitch-averaged loss coefficient. There are greater losses at end-walls (5%-15% and 90%-98% span) than at the midspan. As shown in Figure 8, for the shorter blades of highly loaded helium compressor design, the cascade has very large endwall losses due to leakage flow and corner vortex. The effect of boundary layer on blade is also serious behaved as wake fluid turbulent mixing after the trailing edge of the blade.

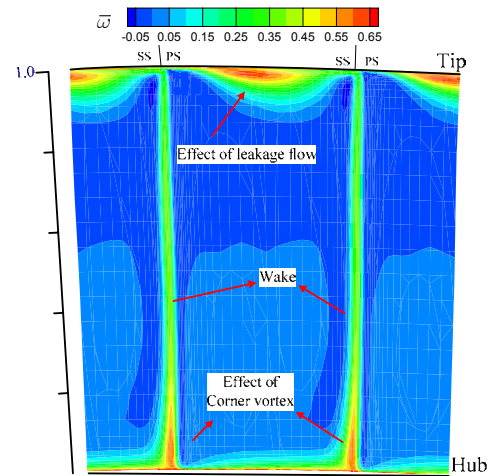


**Figure 8 Total pressure loss coefficient contour at rotor exit**

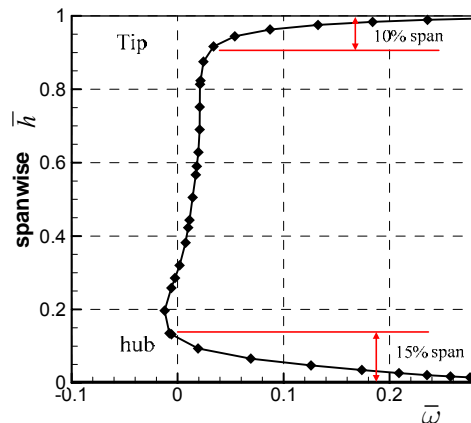


**Figure 9 Pitch-averaged total pressure loss coefficient along blade height at rotor exit**

The passage vortex causes a larger portion of the total pressure loss in turbomachine. The inlet boundary layer, the boundary layers on hub and tip end-walls and the pressure leg of horseshoes vortex are the main components of the passage vortex. The secondary flow vortices occur in any three-dimensional curved channel. From figure 10 we can see that due to the bad flow field at rotor hub and stator shroud, there is a large passage vortex at 50% rotor axial chord in the lower part, which is a stable spiral, locates close to pressure side. At same time, there is an unstable spiral leaning on suction side and shroud end, which is mainly due to the effect of leakage flow. At 50% stator axial chord in the lower part, there exists a little passage vortex near pressure side. A passage vortex with large dimension and intensity appears at upper part.

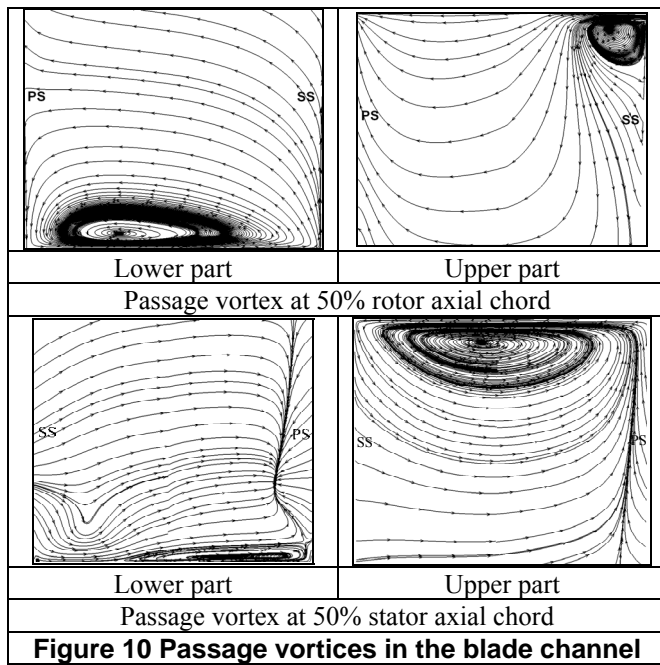


**Figure 10 Passage vortices in the blade channel**

## IMPROVED DESIGN OF THE HIGHLY LOADED HELIUM COMPRESSOR

### The choice of reaction for highly loaded helium compressor stage

How to choose the reaction for a compressor stage is important to its performance. For the helium compressor, it seems that the higher the reaction, the better of its performance is. Such an issue is verified with numerical simulation and discussed as follows.

**Table2 Numerical results of different stage loading and different reaction (Flow coefficient  $\phi = 2.04$ )**

$\Psi=0.63$				
reaction $\Omega$	Pressure ratio $\pi$	Pressure ratio (stagnation) $\pi^*$	Polytropic efficiency $\eta_p$	Rotor efficiency $\eta_{rs}$
0.5	1.029	1.031	82.94	79.81
0.7	1.030	1.031	83.52	85.15
0.9	1.032	1.032	84.30	90.55
$\Psi=0.868$				
0.5	1.041	1.044	86.27	85.72
0.7	1.046	1.055	86.85	87.24
0.9	1.053	1.066	87.29	91.43
$\Psi=1.42$				
0.5	1.070	1.074	88.62	88.84
0.7	1.072	1.075	88.42	89.12
0.9	1.076	1.076	88.38	92.92
1	1.078	1.076	88.22	93.31

$$\left( \eta_p = \frac{R}{c_p} \cdot \frac{\ln(P_2/P_1)}{\ln(T_2/T_1)}, \eta_{rs} = \frac{(P_1/P_0)^{\frac{\gamma-1}{\gamma}} - 1}{T_1/T_0 - 1} : P_0, T_0 \text{ and } P_2, T_2 : \right.$$

The total pressure and temperature at stage inlet and outlet;  $P_0, T_0$ : The static pressure and temperature at stage inlet;  $P_1, T_1$ : The static pressure and temperature at rotor exit)

As shown in table 2, under the conditions of different stage loadings,  $\Psi=0.63, 0.868$  and  $1.42$  respectively, the performances of the helium compressor stage are simulated. The results indicate that the pressure ratio and rotor efficiency increased with the increasing reaction regardless of the loading coefficient. The stage polytropic efficiency will increase for lower loading coefficient  $\Psi=0.63$  and  $\Psi=0.868$ , but will decrease a little for the higher loading coefficient  $\Psi=1.42$ .

Figure 11 shows the pitch-averaged total pressure loss coefficients at the rotor and stator exits for different load coefficients and different reactions. Because of the radial mixing movement of the flow, the total pressure coefficients in some regions are of negative values.

When the load coefficient is 0.63, the stator total loss coefficient varies greater along spanwise than that of the rotor with the same reaction. At rotor exit, the total pressure loss changes a little for different reactions at main flow field about 20%-65% height of blade. While at hub end, the regenerated boundary layers have thickened regardless of the increasing of the reactions. At tip about 15% height of blade, the total pressure loss coefficient increases along with the increasing of reaction progressively. It indicates that the rotor blade load increasing has great influence on tip flow field, thus the loss has increased due to the secondary flow and tip leakage flow. At the stator exit, there is no general trend of the total pressure loss coefficients with the reaction changing. When the reaction increases to 0.9, the stator total pressure losses are of large values, which indicate that the rotor separated flows continue to affecting the stator flow field. The total pressure loss coefficients are of the similar values when reaction is 0.5-0.7. But when reaction increases to 0.9, the curve becomes different from the others.

When load coefficient is 0.868, the total pressure loss coefficients are almost the same at the rotor exit and stator exit for different reactions. At the exit of stator, when reactions are in the range between 0.5 and 0.7, the total pressure losses have nearly the same values from hub to shroud. When reaction increases to 0.9, the total pressure loss coefficient increases at the upper half passage, and decreases at the lower half passage except the area where the total pressure loss coefficient is negative.

When the machine work under highly loaded with the loading coefficient 1.42, the total pressure loss coefficients are not sensitive to reaction at the rotor exit. At stator exit, the total pressure loss coefficients have increased with reaction decreasing from 1.0 to 0.5 in the lower half passage.

In summary, with the load coefficient increasing, the total pressure loss coefficients at rotor exit vary from -0.01 to 0.05; to 0.06 at the stator exit. It shows that the rotor losses would not increase when increasing the load coefficient in helium

compressor. It also shows that the highly loaded design in the paper is feasible, because the increasing of the Mach number is not obvious and the Mach number is still in the subsonic range. The CFD results indicate that stage loading and reaction must be increased together to maintain optimum efficiency.

Generally speaking, the higher reaction is favorable in the helium compressor. For a higher stage loading, the performance of the highly loaded helium compressor improves better for the

high reaction. Therefore the reaction will be chosen as high as 0.9 in our next improved design. Further the simulation results of the total pressure loss coefficients show that it is necessary to reduce and control the developments of end wall boundary layer on the hub and tip end-walls.

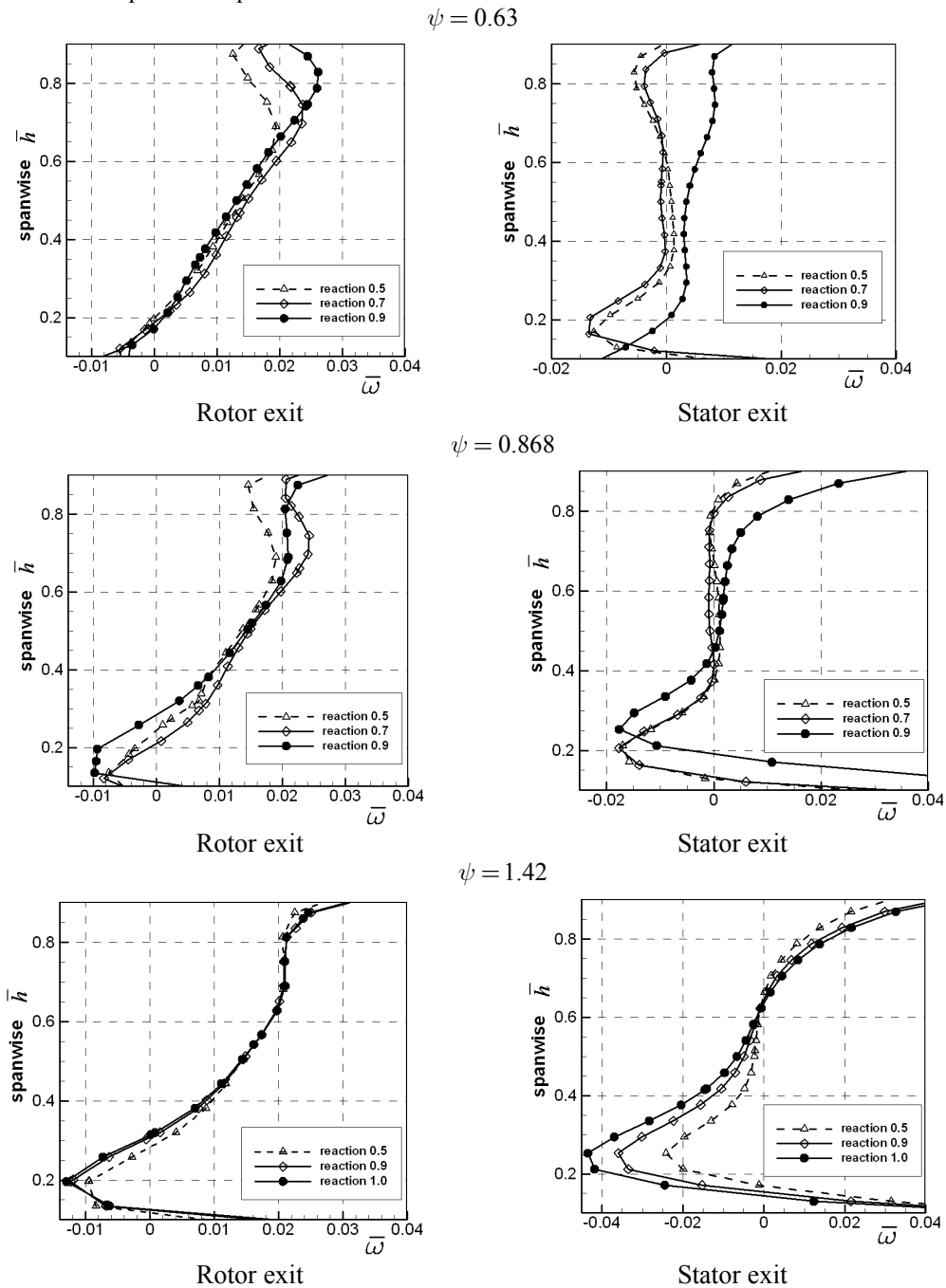


**Figure 11 Distributions of pitch-averaged total pressure loss coefficient along blade height**

### Redistributing spanwise loads

The spanwise swirl distribution (sometimes referred to as the vortex design) is a major contributor to the overall performance of a multistage turbomachine. The changing of the swirl distribution can be considered a 2-D design technique but overall effects can be predicted using three dimensional CFD simulation. In order to reduce the separation at rotor hub, it is necessary to reduce the load at hub section and tip section, and at the same time increase the middle span load in case of ensuring the single stage loading. To keep the rotor inlet swirl, the load redistribution means the rotor outlet swirl has to be redistributed. It is shown in Figure 12, for the preliminary highly loaded design,  $C_{u,r}$  keeps constant both at rotor inlet and at rotor outlet, except at two end-walls. In case 1, the outlet swirl has varied compared with preliminary highly loaded design, shown as black solid triangle line in the figure. From 5%-70% height of blade, the increased swirl has resulted in high turning angle and more load; from 70%-95% height of blade the swirl has decreased in case of serious tip leakage.

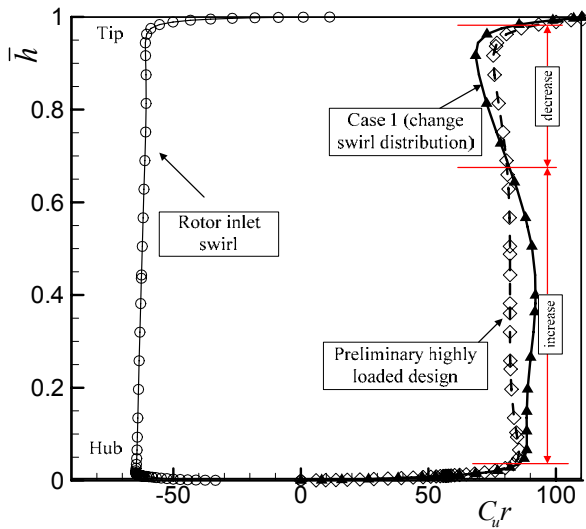


Figure 12 Redistribute spanwise swirls at rotor exit

Figure 13 illustrates the distributions of static pressure and separation regions on rotor suction surfaces for preliminary design and case 1.

The static pressure pattern changed with the outlet swirl improved. Although the three dimensional separation areas do not decrease obviously, the start location of separation line moves back at axial flow direction.

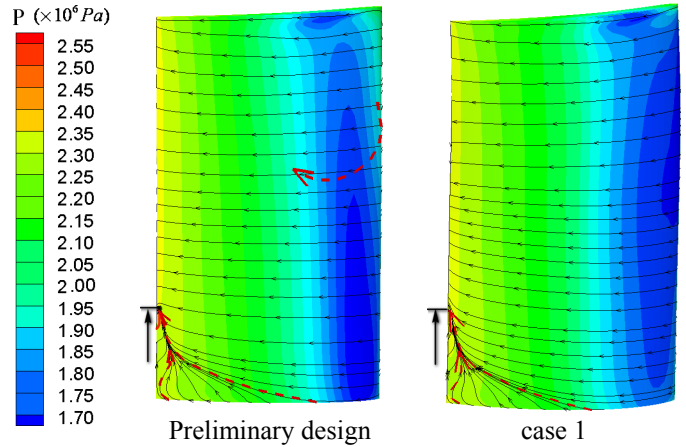


Figure 13 Contours of static pressure and streamline on rotor suction surfaces

The velocity circulation re-distribution at the outlet affects the loading at each section. From the static pressure coefficient distribution at 15% height of blade, it is seen that, both the inlet angle of incidence and the load at leading edge have decreased; the minimal pressure point has risen on suction side. And also the pressure gradient drops down within the range between 10% and 50% chord, thus the development of boundary layer on blade surface has been controlled. At pressure side, the static pressure reduces within the range between 10% and 30% chord. From the static pressure distribution at 50% height of blade, it can be seen that the loading has increased between 0% and 50% chord region. And the static pressure increases at the leading edge of pressure side making the curve smoother, at the same time the negative pressure gradient on the suction surface has decreased a little between 10% and 40% chord, so the increasing load at middle span do not thicken the boundary layer on blade surface. At the position of 80% blade span, both the positive incidence angle and the load near the leading edge increased. The static pressure at the pressure surface increases before the 25% position and decreases slightly after the 25% position; the static pressure at the suction surface decreases before the 20% position and increases between 20% and 60% chord. The lowest pressure point moves forward. And the negative pressure gradient of the suction surface increases slightly, which will affects the flow field on shroud area. However, after the 60% chord, the difference between the pressure surface and suction surface decreases, the intensity of passage secondary flow has weakened. It indicates that, the static pressure coefficient of blade surface is improved when decreasing the work at shroud end.

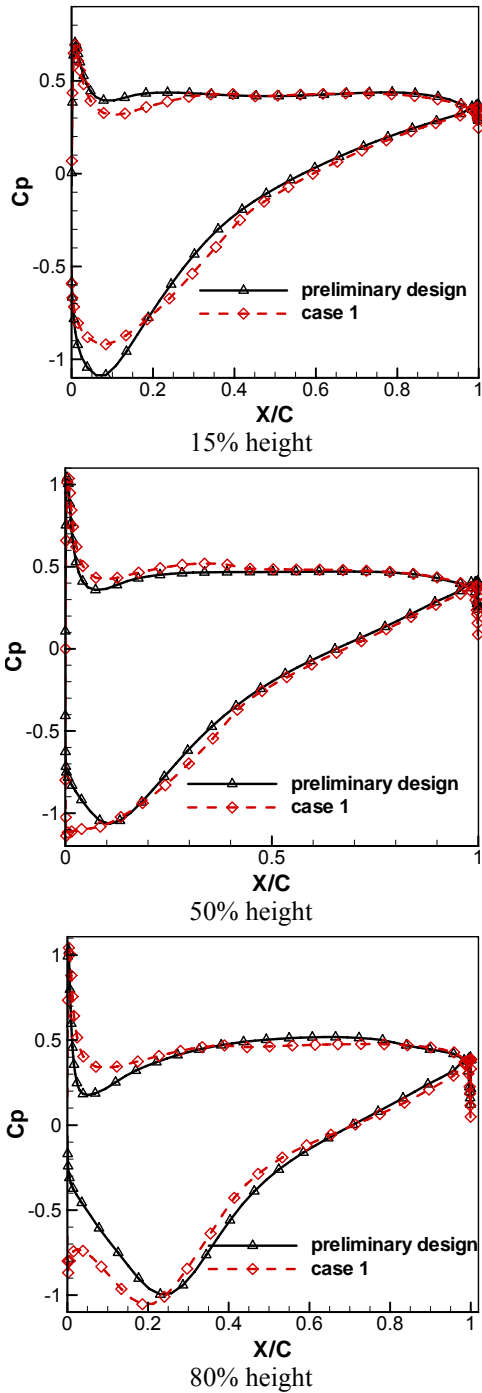


Figure 14 Static pressure coefficient distributions

**Maximum thickness position**

The maximum thickness of the helium compressor blade profile is different from that of air compressor as indicated by Yanli Long in two-dimensional profile analysis<sup>[13]</sup>. Here we try to investigate the maximum thickness effects on the three-dimensional flow field of the helium compressor blade. The three-dimensional profiling can improve the aerodynamic performance of the helium compressor. In order to discuss the relationship between the maximum thickness and the

aerodynamic performance of the helium compressor, two cases have been analyzed here. The above preliminary highly loaded design and case 1 have the same thickness stacking, which has the maximum thickness of 10% chord at the hub, 8% chord at the tip, and a linear change in the middle part.

Compared with case 1, two other cases have been presented: the maximum thickness is 9% chord at the hub and 7% at the tip, with a linear change in the middle part (named as case 2); second, the maximum thickness is 12% chord at the hub and 10% at the tip, with a linear change in the middle part (named as case 3). Three-dimensional flow fields were numerically simulated for these types of helium compressor cascades.

**Table 4 The computation result**

	Static pressure ratio $\pi$	Pressure ratio stagnation $\pi^*$	Isentropic efficiency $\eta_s$
Case 1	1.068	1.078	88.56
Case 2	1.070	1.080	88.90
Case 3	1.067	1.077	88.02

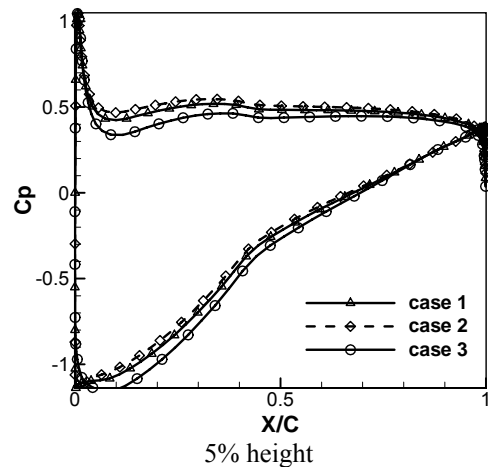
Note: efficiency is defined as:

$$\eta_s = \frac{(\pi^*)^{\frac{k-1}{k}} - 1}{\frac{T_2^*}{T_0^*} - 1}$$

As shown in Table 4, when decreasing the maximum ratio of the airfoil thickness from hub to tip (case 2), both the total pressure ratio and isentropic efficiency are increased.

**1. Static pressure coefficient distribution**

As shown in Figure 15, the surface static pressure coefficient distribution of case 2 shows a reduction in blade force and an increase in effective incidence near the end-wall, and the static pressure distribution becomes more favorable, and the inverse pressure gradient is controlled, while case 3 shows the opposite trend. Similar observations can be made at the rotor mid-span. But at the leading edge of the rotor tip, case 2 causes an increase in blade force and a reduction in incidence. The opposite trends are observed for case 3. This means that at the rotor tip, the thickness needs some further modification compared with case 3.



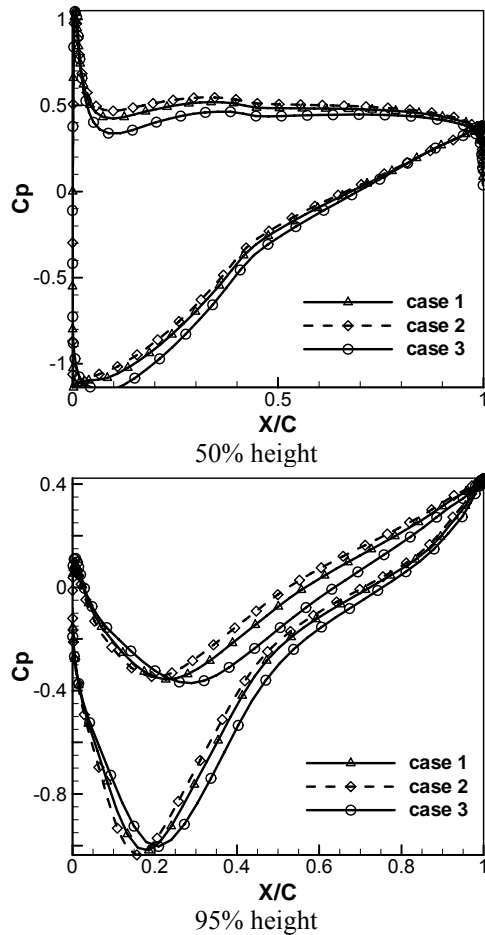


Figure 15 Sstatic pressure coefficient distributions

## 2. Three-dimensional separation in corner

Regions of three dimensional separations have been identified as an inherent flow feature of the corner formed by the suction surface and end-wall of axial compressors.

Following the observation of the figure 16, it can be seen that the leading edge horse-shoe vortex and its associated dividing streamlines that start from the leading edge stagnation (saddle  $S_1$ ) point, which form the base of the vortex system, play a major role in the mechanism of 3D separation.

The streamlines shown in Fig.16 can reveal the leading edge saddle point of separation and the corresponding nodal point of attachment labeled ( $N_1, S_1$ ). Also observable on the endwall corner is the point at which the suction side leg of the dividing streamline (which forms the base of the horse-shoe vortex) interacts with the suction surface. Comparing the suction surface and endwall limiting streamline patterns computed for the case 1 and case 2, as might be expected, an increase in the chordwise of the separated region from the leading edge and the spanwise extent from the endwall is evident in case 1. The hub separation line on case 1 blade suction surface has started earlier nearly 10% of chordwise, and the suction surface separation line has extended 10% more in spanwise than case 2.

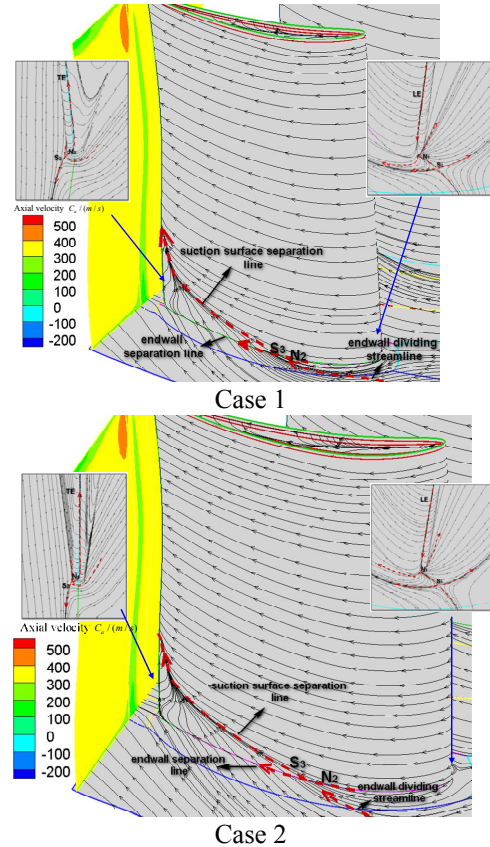


Figure 16 Endwall corner streamlines and contours of calculated axial velocity (m/s) in the trailing edge plane

Close inspections of the endwall/suction surface corner suggests that this point takes the form of a multiple critical point (node  $N_2$  on the endwall and a saddle point  $S_3$  on the suction surface). The trailing edge saddle point  $S_2$  on the endwall, acts as a division between the limiting streamlines undergoing flow reversal on the suction surface corner and those proceeding normally. At trailing edge the difference between case 1 and case 2 is not evident, while the saddle point  $S_2$  seems appears earlier in case 2 than in case 1. The calculated axial velocity in the trailing edge plane has also been shown in figure 16. There are high axial velocity regions (nearly 500m/s) at the tip trailing edge, maybe caused by the tip leakage losses. Comparing these two regions, the one in case 1 is a little bigger than that in case 2, which means more serious tip loss.

## 3. Total pressure loss coefficient

As shown in figure17, the total pressure losses accumulate at hub end. Comparing the three cases, case 2 reduces the size of the high loss region significantly, and the peak value of the loss core also reduces remarkably.

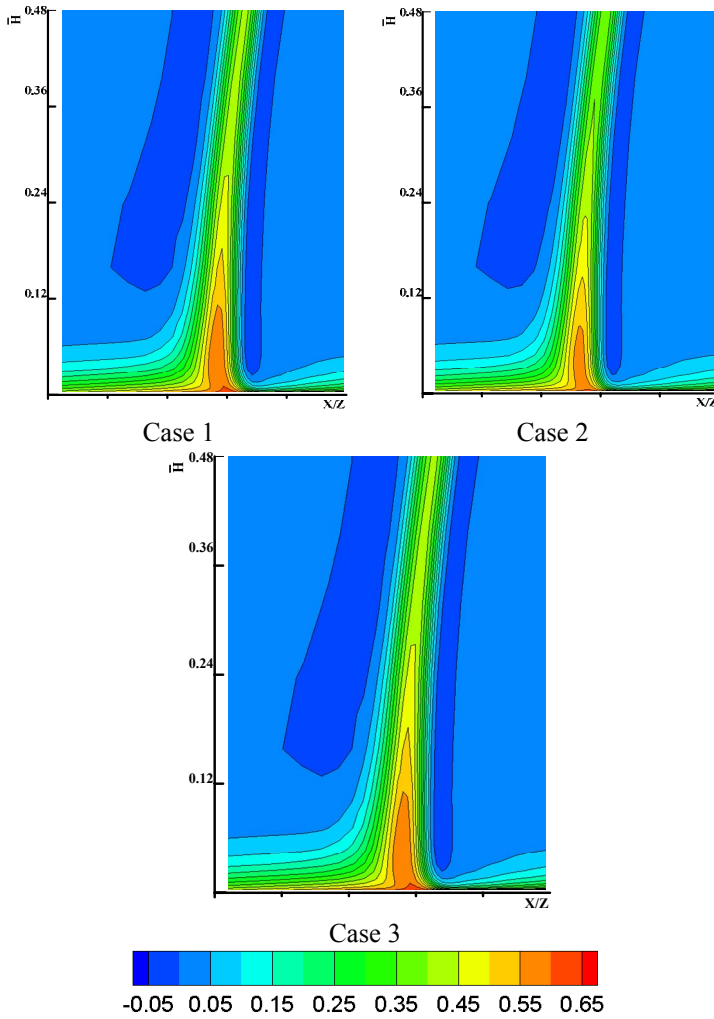


Figure 17 Lower half span of the total loss coefficient contours at rotor exit

### OVERALL PERFORMANCE

The single stage performance at design rotational speed is obtained by analyzing the compressor stage at different back pressure. We plot the characteristic curves as shown in figure 18, which are the curves of pressure against helium flow and stage isentropic efficiency against helium flow.

Comparing the preliminary highly loaded design and the final improved one, case 2, the pressure ratio and isentropic efficiency are both increased, which indicates the improved design has reduced the three-dimensional separation including passage vortex and tip vortex, thus increased the cascade diffusion ability and also the stable operating range.

Comparing the prototype one and case 2, the stage pressure ratio has increased obviously due to higher stage loading, but the stage efficiency does not drop a lot, even a little larger than prototype one at design point. With the flow rate reduced, the efficiency increased in prototype more rapidly than that of the case 2 until near the stall angle of attack is reached. It is shown that the stable operating range has decreased a little due to highly loaded design.

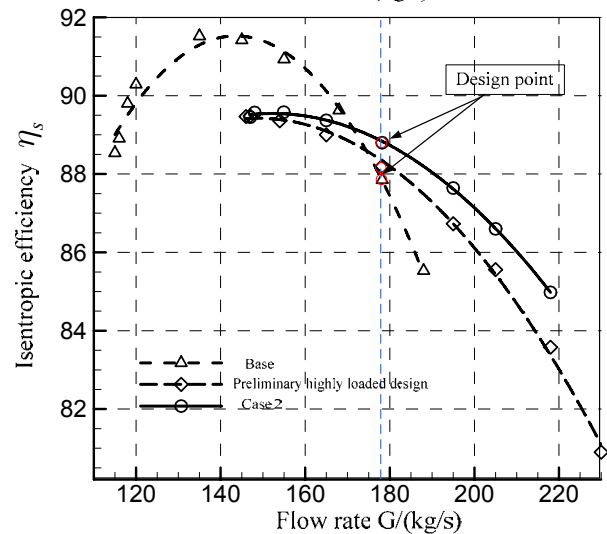
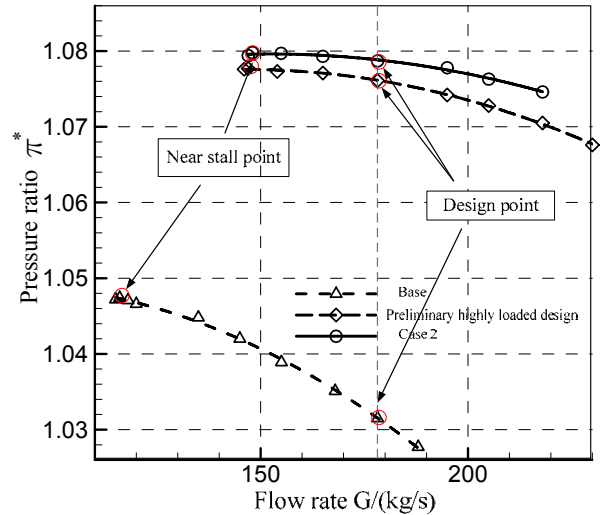


Figure 18 Performance curves at design speed (simulation)

### CONCLUSIONS

The following observations can be made from this study:

1. The new helium compressor triangle velocity with large axial velocity is feasible in the three dimensional highly loaded design. The stage loading is increased 3 times; as a result, the helium compressor stage numbers decrease from 16 to 6 and the efficiency is acceptable.
2. The relationship between stage loading and reaction of helium compressor has investigated for the high performance aerodynamic design. It was found that a larger reaction is favorable to get the expected pressure ratio and efficiency.
3. It is necessary to control the three dimensional separation to increase the stage efficiency and pressure ratio by three dimensional improved design. Redistribute radial compression work is one of the techniques to improve the performance.
4. The proper distribution of the ratio of the maximum airfoil thickness to chord from hub to tip, or say, three

dimensional profiling, has great effects on the flow of highly loaded helium compressor.

5. Although the stage loading has increased a lot, the stall margin of the designed highly loaded helium compressor is acceptable comparing to the prototype design.

## NOMENCLATURE

$P$  : Pressure

$\rho$  : Helium density

$W$  : Relative velocity magnitude

$U$  : Blade speed

$C$  : Absolute velocity magnitude

$L_u$  : Stage loading

$\Delta W_u$  : Change of tangential gas velocity

$C_u$  : Absolute velocity on peripheral velocity

$r$  : Radial axis

$\tau$  : Solidity (chord/pitch)

$\Omega$  : Reaction

$\varphi$  : Flow coefficient

$\psi$  : Load coefficient

$\alpha$  : Absolute flow angle

$\beta$  : Relative flow angle

$\bar{\omega} = (P_0 - P) / P_{v0}$   $P_{v0}$  : The dynamic pressure at cascade inlet.

$Cp = (P - P_{inlet}) / (0.5 \rho_{inlet} W_{inlet}^2)$

S: saddle

N: node

TE: trailing edge

LE: leading edge

S.S: suction surface

P.S: pressure surface

## Subscript

0: mass-averaged rotor inlet

1: mass-averaged stator inlet

2: mass-averaged stator inlet

a: axial component

## ACKNOWLEDGEMENT

The authors would like to acknowledge the support of China Doctoral Grant No. 20092304110004.

## REFERENCES

- [1] Matzner, D., 2004, "PBMR project status and the way ahead", In: Proceedings of the 2nd International Topical Meeting on High Temperature Reactor Technology, Beijing, China.
- [2] Kostin, V. I., Kodochigov, N. G., et al, 2004, "Power conversion unit with direct gas-turbine cycle for electric power generation as a part of GT-MHR Reactor Plant", In: Proceedings of the 2nd International Topical Meeting on High Temperature Reactor Technology, Beijing, China.

- [3] Kunitomi, K., Yan, X., et al, 2004, "GTHTR300C for hydrogen cogeneration", In: Proceedings of the 2nd International Topical Meeting on High Temperature Reactor Technology, Beijing, China.
- [4] Muto, Y. et al, 1998, "Present Activity of the Feasibility Study of HTGR-GT System", IAEA Technical Committee Meeting, INET Beijing.
- [5] Muto, Y. et al, 1999, "Design Study of Helium Turbine for the 600MWt HTGR-GT Power Plant", International Gas Turbine Congress, Kobe.
- [6] Muto, Yasushi, et al, 2000, "Design Study of Helium Turbine for the 300MW HTGR-GT Power Plant", ASME Turbo Expo, 2000.
- [7] GCRA, 1994, "Evaluation of the Gas Turbine Modular helium Reactor", DOE-GT-MHR-100002.
- [8] Van den Braembussche, R.A., Brouckaert, J.F., 2008, "Design and optimization of a multistage turbine for helium cooled reactor". Nuclear Engineering and Design.
- [9] Muto, Yasushi, 2001, "Improvement in the Design of Helium Turbine for the HTGR-GT Power Plant". ASME Turbo Expo.
- [10] Yan, X., Takizuka, T., Kunitomi, K. 2008, "Aerodynamic design, model test, and CFD analysis for multistage axial helium compressor", Journal of Turbomachinery.
- [11] Wisler, D. C., 1985, "Loss Reduction in Axial-Flow Compressors through Low-Speed Model Testing," ASME J. Eng. Gas Turbines Power, 107, pp. 354-363.
- [12] Mihayiluofu, A.И., Baolisuofu, B.B., Kalining, Э.К., 1964, "Closed Cycle Gas Turbine Plant", Science Publishing Company, pp.39-57.
- [13] Long, Yanli and Xu, Limin, 2008, "Simulation for New Cascade of Helium Compressor with Enhanced Pressure Ratio," ASME Turbo Expo GT2008-50690.
- [14] Tony Dickens, Ivor Day, 2009, "The design of highly loaded axial compressors," ASME Turbo Expo GT2009-59291.
- [15] Ke, Tingfeng and Zheng, Qun, 2010, "The Highly Loaded Aerodynamic Design and performance enhancement of a Helium Compressor", ASME Turbo Expo GT2010-23116, June 14-18.